

# Nonequilibrium interactions between two quantum circuits

V S Khrapai<sup>1,2</sup>, S Ludwig<sup>1</sup>, J P Kotthaus<sup>1</sup>, H P Tranitz<sup>3</sup> and W Wegscheider<sup>3</sup>

<sup>1</sup> Center for NanoScience and Department für Physik, Ludwig-Maximilians-Universität, Geschwister-Scholl-Platz 1, D-80539 München, Germany

<sup>2</sup> Institute of Solid State Physics RAS, Chernogolovka, 142432, Russian Federation

<sup>3</sup> Institut für Experimentelle und Angewandte Physik, Universität Regensburg, D-93040 Regensburg, Germany

E-mail: [dick@issp.ac.ru](mailto:dick@issp.ac.ru) (V S Khrapai)

Received 6 May 2008, in final form 30 September 2008

Published 23 October 2008

Online at [stacks.iop.org/JPhysCM/20/454205](http://stacks.iop.org/JPhysCM/20/454205)

## Abstract

We briefly overview our recent results on nonequilibrium interactions between neighbouring electrically isolated nanostructures. One of the nanostructures is represented by an externally biased quantum point contact (drive-QPC), which is used to supply energy quanta to the second nanostructure (detector). Absorption of these nonequilibrium quanta of energy generates a dc current in the detector, or changes its differential conductance. We present results for a double quantum dot, a single quantum dot or a second QPC placed in the detector circuit. In all three cases a detection of quanta with energies up to  $\sim 1$  meV is possible for bias voltages across the drive-QPC in the mV range. The results are qualitatively consistent with an energy transfer mechanism based on nonequilibrium acoustic phonons.

(Some figures in this article are in colour only in the electronic version)

## 1. Introduction

Present GaAs fabrication techniques enable one to create a pair of nanostructures connected to separate two-dimensional electron gas (2DEG) leads and placed just about 100 nm apart. Out of thermodynamic equilibrium a net transfer of energy between such two quantum circuits can occur. This can happen both directly via a Coulomb interaction between the electrons of the two circuits, and indirectly via emission/absorption of energy quanta into/from their common environment. In the last case, exchange with the quanta of the electromagnetic field (photons) as well as those of the crystal lattice vibrations (phonons) is possible thanks to electromagnetic and electron-phonon interactions. Recent experiments [1–3] gave no definite answer on what determines the dominant interaction mechanism in similar devices. It is important to know this, for example, for the application of coupled nanostructures in quantum measurements.

Regardless of the type of interaction, the change of the energy and momentum of an electron satisfies the conservation laws, which can impose constraints on the respective energy transfer mechanism. These constraints are most crucial

for freely moving electrons. For Coulomb interaction, for example, the conservation of momentum determines a positive sign of the Coulomb drag between clean one-dimensional (1D) quantum wires [4] and parallel 2DEGs in bilayer systems [5]. Emission/absorption of an energy quantum from the environment by a 2DEG electron is possible provided the velocity  $v$  of the corresponding particle (a photon or an acoustic phonon here) is smaller than the electron's Fermi velocity  $v < v_F$  [6]. This condition is only fulfilled for acoustic phonons thanks to a small sound velocity ( $v_s \ll v_F$  in typical 2DEGs). Conservation laws allow the interaction with acoustic phonons of in-plane momenta as high as  $2k_F$  and corresponding energies up to  $2\hbar k_F v_s \sim 1$  meV, where  $k_F$  and  $\hbar$  are, respectively, the Fermi momentum in the 2DEG and Planck's constant. No strict constraints exist for confined electrons because of a lack of momentum conservation. Hence, the electrons in a quantum dot (QD) can interact both with microwave photons [7, 8] and acoustic phonons [9].

In this paper we overview a set of experiments (partly reported in [2, 10, 11]) on nonequilibrium interactions between neighbouring electrically isolated nanostructures laterally defined within the 2DEG beneath the surface of a

GaAs/AlGaAs heterostructure. Compared to previous work, we present new experimental data and extend a microscopic discussion of the observations. The AFM micrograph of the sample is shown in figure 1(a). The negatively biased central gate C depletes the underlying 2DEG and divides the sample into two coplanar nanostructures, defined and controlled by voltages on gates 1–10, with four separately contacted 2DEG leads (marked by crossed squares in figure 1(a)). One of the nanostructures is an externally biased quantum point contact (drive-QPC) and is used to supply energy to the second nanostructure (detector). Absorption of energy results in generation of a dc current in the detector circuit or changes its differential conductance, which can be measured in the experiment. The energy spectrum of the excitation as well as its spatial asymmetry are studied by using a double quantum dot (DQD) (figure 1(b)), a second QPC (figure 1(c)) or a single QD (figure 1(d)) as the detector. In all three cases the detection of quanta with energies up to  $\sim 1$  meV occurs for bias voltages across the drive-QPC ( $V_{\text{DRIVE}}$ ) in the mV range. As shown below, our observations demonstrate that the drive-QPC provides a strong spatially asymmetric excitation to the electrons of the 2DEG leads of the detector. This strongly suggests that the dominant energy transfer mechanism between the two quantum circuits in our experiment is based on emission/absorption of nonequilibrium acoustic phonons happening in the 2DEG leads of the drive/detector nanostructure. This mechanism has to be considered in experiments on coupled quantum circuits, at least in the regime of high external bias.

This paper is organized as follows. The details of the experiment are described in section 2. In the subsequent sections the results for three detector realizations are presented. In section 3 we describe the experiment with the DQD-detector, which provides a quantitative measure for the drive-QPC-mediated excitation bandwidth. Observation of a so-called counterflow effect [10] with the detector-QPC is described in section 4. A qualitative analogy as well as a strong quantitative difference of the results to thermopower experiments in single QPCs [12, 13] are given in this section. Excitation of discrete energy levels in the QD-detector mediated by the drive-QPC is reported in section 5. The discussion of the observations in terms of a phonon-mediated energy transfer mechanism between the two circuits is given in the last section 6.

## 2. Experimental details

All the measurements presented below were performed on a GaAs/AlGaAs heterostructure, containing a 2DEG 90 nm below the surface, with a carrier density of  $2.8 \times 10^{11} \text{ cm}^{-2}$  and a low-temperature mobility of  $1.4 \times 10^6 \text{ cm}^2 \text{ V}^{-1} \text{ s}^{-1}$ . The metallic gate layout of figure 1(a) was designed by means of e-beam lithography. The sample was immersed in the mixing chamber of a dilution refrigerator with a base temperature of 25 mK and cooled down to an electron temperature below 150 mK. DC or low frequency (21 Hz) ac current measurements in the drive and detector circuits were performed by use of two current–voltage converters

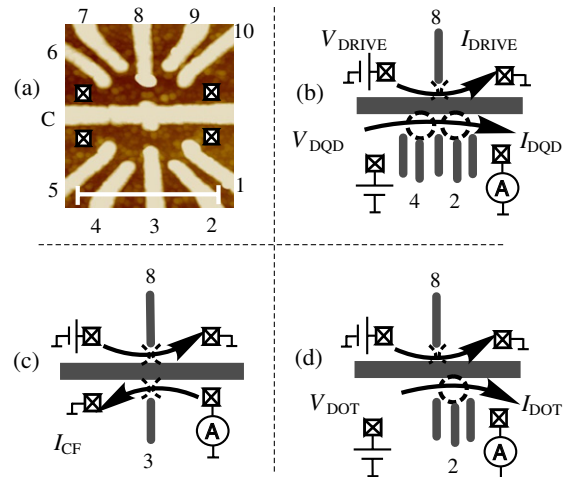


**Figure 1.** (a) AFM micrograph of the nanostructure. Metal gates on the surface of the heterostructure are shown as bright. Crossed squares mark contacted 2DEG regions. The scale bar equals  $1 \mu\text{m}$ . (b), (c), (d) Sketches of the measurement configuration for three different realizations of the detector nanostructure. Gates used in each case are shown as dark.

with variable gain from  $10^6$  to  $10^9$  V/A followed by a digital voltmeter or a lock-in amplifier, respectively. The lock-in technique was particularly useful for low-impedance counterflow measurements (see section 4), where the dc signal to noise ratio was poor. In some cases, a differential signal was obtained by numerically deriving the dc current data (section 5) or the dc data were obtained via numerical integration of the ac signal (section 4). We have carefully checked that these procedures are equivalent in the regime of the nearly pinched-off detector-QPC. Careful check for the absence of the leakage between the two circuits, measurements with interchanged signal and ground ohmic contacts, interchanged drive and detector nanostructures, as well as simultaneous dc and ac measurements, were performed to ensure the small signals measured are free from spurious effects.

## 3. Double-dot quantum ratchet

In this section we describe the experiment with a DQD in the detector circuit [2]. A sketch of the measurement is shown in figure 1(b). Two serially connected QDs with weak interdot coupling ( $t \sim 0.1 \mu\text{eV}$ ) and strong dot–lead coupling ( $\Gamma \approx 40 \mu\text{eV}$ ) are formed on one side of the gate C by negatively biased gates 1–5. Typical values of charging energy, single-particle level spacing and interdot Coulomb energy are, respectively 1.5 meV,  $100 \mu\text{eV}$  and  $100\text{--}200 \mu\text{eV}$ . The charge configuration of the DQD is controlled by voltages  $V_2, V_4$  applied to gates 2 and 4, which predominantly couple to the electrochemical potentials of the right and left QD, respectively. A small bias voltage across the DQD  $V_{\text{DQD}} = -20 \mu\text{V}$  is applied throughout the experiment.

In the absence of current in the drive circuit ( $V_{\text{DRIVE}} = 0$ ),  $I_{\text{DQD}}$  is mainly suppressed because of the Coulomb blockade (figure 2(a)). The only exception is a pair of sharp resonances in the  $[V_2, V_4]$  plane (the so-called stability diagram), where

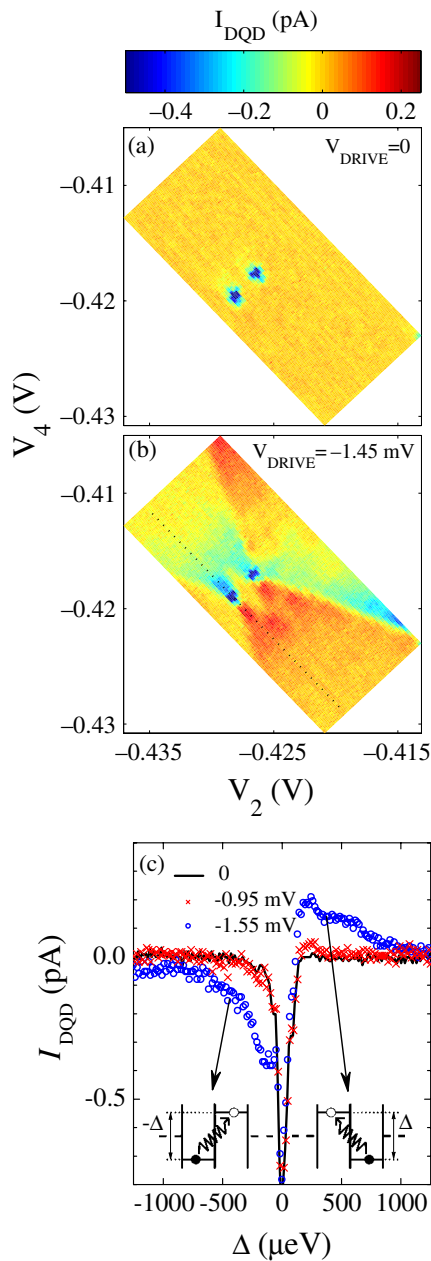


**Figure 2.** (a), (b) Scale-bar plot of  $I_{\text{DQD}}$  for two corresponding values of  $V_{\text{DRIVE}}$ . The top colour bar is the same for both panels. (c)  $I_{\text{DQD}}$  versus the electrochemical potential difference between the two dots, taken along the dashed trace in (b) for three values of  $V_{\text{DRIVE}}$ . The left/right inset schematically shows the inelastic interdot tunnelling processes responsible for a negative/positive ratchet contribution to  $I_{\text{DQD}}$ . Figure (c) is reproduced with permission from [11] with minor changes to axes scales.

the electrochemical potentials of both dots  $\mu_R, \mu_L$  and 2DEG leads are aligned [14].

The situation changes drastically at finite bias across the drive-QPC, tuned halfway between the pinch-off and first conductance plateau ( $g_{\text{DRIVE}} \equiv dI_{\text{DRIVE}}/dV_{\text{DRIVE}} \approx 0.5 G_0$ , where  $G_0 = 2e^2/h$  is the conductance quantum). In figure 2(b)  $I_{\text{DQD}}$  is plotted throughout the same region of the stability diagram for  $V_{\text{DRIVE}} = -1.45$  mV. In contrast to figure 2(a), a non-zero current now flows across the DQD in the regions of

stable ground state charge configurations. The sign of the DQD current depends on the position in the stability diagram relative to the resonances. The current is negative on the left and above the resonances and positive on the right and below them ( $I_{\text{DQD}} > 0$  corresponds to electrons moving to the left-hand side in the lower circuit of figure 1(b)).  $I_{\text{DQD}}$  changes abruptly at the boundaries of stable ground state configurations, making them visible in figure 2(b) (nearly horizontal and vertical lines originating from resonances, see [2] for details). Note that such a behaviour is observed around many pairs of resonances in the stability diagram [11].

All the main features of figure 2(b) can be explained by inelastic interdot tunnelling in the DQD, mediated by resonant absorption of an energy quantum from the drive-QPC circuit, similar to photon-assisted tunnelling [14]. The energy absorbed by the topmost DQD electron initially localized in one dot compensates for the difference of the dots' electrochemical potentials  $\Delta \equiv \mu_L - \mu_R$  and lifts the Coulomb blockade of interdot and dot-lead tunnelling (see the insets of figure 2(c)). This picture is further supported by the observed suppression of  $I_{\text{DQD}}$  inside a small diamond-shaped region between the resonances (figure 2(b)). There, the excited state configuration is stable with respect to dot-lead tunnelling so that absorption of energy does not result in  $I_{\text{DQD}}$  [2].

Owing to the spatial asymmetry of the quantized charge distribution the DQD represents a realization of a quantum ratchet system [15] capable of rectifying nonequilibrium fluctuations in the environment. The resonant character of the rectification can be used for spectrometry of the excitation provided by the drive-QPC. In figure 2(c) we plot  $I_{\text{DQD}}$  as a function of  $\Delta$  along the dashed trace in the stability diagram of figure 2(b) for a set of  $V_{\text{DRIVE}}$  values (gate voltage to energy is converted with a standard calibration procedure [14]). At  $|V_{\text{DRIVE}}| \gtrsim 1$  mV the ratchet contribution to  $I_{\text{DQD}}$ , which is odd in  $\Delta$ , sets in within about a 1 meV wide energy band  $|\Delta| \lesssim 1$  meV.

Obviously, the energy transferred to the detector circuit is a part of the Joule heat dissipated in the drive circuit. However, the efficiency of this energization turns out to be a nonmonotonic function of the drive-QPC conductance. In figure 3(a) we show a colour-scale plot of  $I_{\text{DQD}}$  as a function of  $V_{\text{DRIVE}}$  and gate voltage  $V_8$ , which controls the drive-QPC conductance (figure 1(b)). Here,  $\Delta = -450 \mu\text{eV}$ . For comparison, a derivative of the drive-QPC conductance with respect to its gate voltage (below referred to as transconductance,  $g_{\text{DRIVE}}^T = dg_{\text{DRIVE}}/dV_8$ ) is shown for identical axes in figure 3(b). In both figures, the dashed lines mark the boundaries between the so-called 0.5-plateaus on the nonlinear differential conductance ( $g_{\text{DRIVE}} \approx G_0/2$ ) and its pinch-off and first plateau ( $g_{\text{DRIVE}} \approx G_0$ ). The plateaus and the boundaries between them appear as regions of low and high transconductance in figure 3(b) [16]. As follows from figure 3(a), at fixed  $V_{\text{DRIVE}}$   $I_{\text{DQD}}$  is maximal on the drive-QPC 0.5-plateau and suppressed on its first conductance plateau. In other words, the energization of the DQD ratchet is strong (weak) when the drive-QPC is tuned to a strongly nonlinear (almost linear) transport regime. Note that a similar, though much less developed, maximum of the energization efficiency

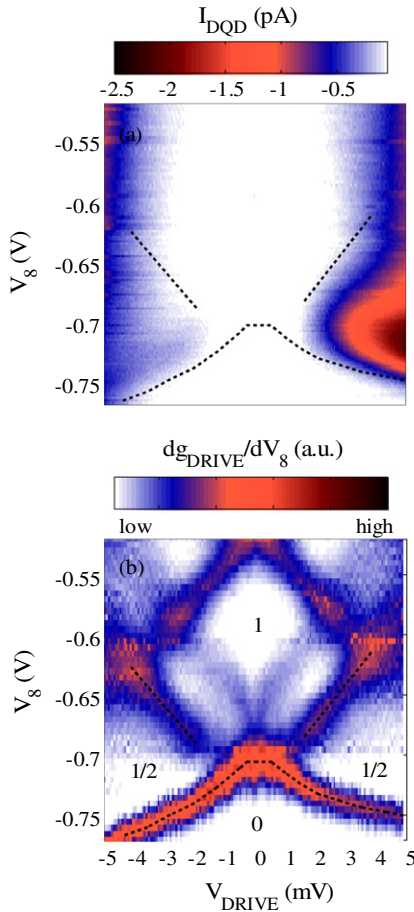


**Figure 3.** (a) Colour (grey-scale) plot of  $I_{\text{DQD}}$  versus bias and gate voltage of the drive-QPC. (b) Colour (grey-scale) plot of  $g_{\text{DRIVE}}^{\text{T}}$  for the same region of the  $[V_{\text{DRIVE}}, V_8]$  plane. Low  $g_{\text{DRIVE}}^{\text{T}}$  regions are marked by corresponding approximate values of  $g_{\text{DRIVE}}/G_0$ . In both figures dashed guidelines mark the boundaries of half-integer plateaus on  $g_{\text{DRIVE}}$ .

can be observed in the region of the drive-QPC 1.5-plateau at not too high bias [2].

#### 4. Counterflow of electrons in isolated QPCs

In section 3 we demonstrated that a broad-band energy transfer from the drive-QPC to the neighbouring circuit can be detected with a quantum ratchet system. Here we analyse this energy flow, placing a second QPC (detector-QPC) in the detector circuit, which represents a quantum system with no spatial asymmetry [10]. Both drive/detector QPCs have a one-dimensional (1D) subband spacing of about 4 meV/3 meV, while the half-width of the transition region between the quantized plateaus is  $\delta \approx 0.5$  meV. Throughout this section we keep  $g_{\text{DRIVE}} \approx 0.5 G_0$ , which corresponds to the most pronounced effect. The sketch of the experiment is given in figure 1(c). The current generated in the unbiased detector circuit is measured as a function of  $V_{\text{DRIVE}}$  or gate voltage  $V_3$ , which controls the position of the 1D subbands of the detector-QPC relative to the Fermi energy  $E_{\text{F}}$  of its 2DEG leads (thereby tuning its linear response conductance  $G_{\text{DET}}$ ).

The detector current versus  $V_{\text{DRIVE}}$  is plotted in figure 4 for two values of  $V_3$ , which correspond to a position of the

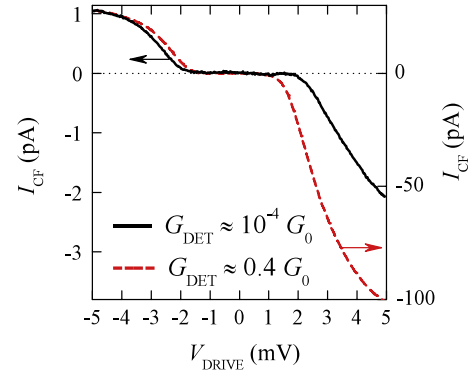


**Figure 4.** Current through the detector-QPC as a function of bias across the drive-QPC. The data for two indicated values of the detector-QPC conductance are plotted on corresponding left and right ordinate scales.

lowest 1D subband bottom  $E_0$  well above  $E_{\text{F}}$  or almost aligned with it. At high enough  $|V_{\text{DRIVE}}|$  a finite current is measured, which is positive/negative for  $V_{\text{DRIVE}} < 0 / > 0$ , i.e. it flows in the direction opposite to that of  $I_{\text{DRIVE}}$ . Below we refer to this current as a counterflow current  $I_{\text{CF}}$ . Note that  $I_{\text{CF}}$  increases as  $E_0$  approaches  $E_{\text{F}}$  from above, although much slower than the relative increment of  $G_{\text{DET}}$ . In figure 5(a) we compare the dependences of  $G_{\text{DET}}$  and  $I_{\text{CF}}$  on  $V_3$  in a wide range of gate voltages between the pinch-off and fully opened detector-QPC. The increase of  $G_{\text{DET}}$  is accompanied by strong oscillations of  $I_{\text{CF}}$ , which displays three well-developed maxima before the detector-QPC is opened completely. The positions of maxima correspond to half-integer conductance values  $G_{\text{DET}} \approx (i + 1/2)G_0$  attained each time the bottom of the  $i$ th 1D subband  $E_i \propto -|e|V_3$  ( $i = 0, 1, 2$ ) aligns with  $E_{\text{F}}$ .

Oscillations of  $I_{\text{CF}}$  are reminiscent of well-known oscillations of thermopower in single QPCs [12, 13]. In the absence of thermal equilibrium, the energy balance between the 2DEG leads of the detector-QPC is broken which results in net electric current:

$$I = \frac{2e}{h} \sum_i \int [f_{\text{R}}^i - f_{\text{L}}^i] T_i dE. \quad (1)$$

Here,  $f_{\text{R}}^i(E)$  ( $f_{\text{L}}^i(E)$ ) is the average occupancy of the left (right) moving electron states in the right (left) 2DEG lead of the detector-QPC at energy  $E$  [17]. In thermopower experiments these are just Fermi–Dirac distributions with appropriate temperatures. The energy dependence of the  $i$ th subband transmission probability evaluated in a saddle-point approximation [17] is given by  $T_i = 1/(1 + \exp((E_i - E_{\text{F}})/\delta))$ , where  $\delta$  is a half-width of the energy window corresponding to  $0.25 < T_i < 0.75$ . At temperatures low compared to  $\delta$  thermoelectric current is proportional to  $\sum dT_i/dE_i$ , i.e. it oscillates as the QPC transconductance. The shape of the oscillations of  $I_{\text{CF}}$  in figure 5(a) is indeed close to that of  $g_{\text{DET}}^{\text{T}}$  (solid line)<sup>4</sup>. This

<sup>4</sup> A poor comparison between  $I_{\text{CF}}$  and  $g_{\text{DET}}^{\text{T}}$  for the left-most peak in figure 5(a) is related to the so-called 0.7 anomaly in detector conductance, which causes the asymmetry of the  $g_{\text{DET}}^{\text{T}}$  peak. This effect is usually attributed to interactions, hence the single-particle approximation to thermopower is not likely to be accurate in this region.

indicates that the counterflow effect is related to energetic imbalance between the two 2DEG leads of the detector-QPC. Note that a sign change of  $I_{CF}$  on the second quantized plateau could be ascribed to a slightly nonmonotonic behaviour of  $G_{DET}$  in this region (i.e.  $g_{DET}^T < 0$ ).

Despite this qualitative analogy, we find a remarkable quantitative disagreement between the thermoelectric model and experiment. In figure 5(b) the counterflow data and  $g_{DET}^T$  are plotted on a logarithmic scale near the pinch-off ( $E_0 \gg E_F$ ), where both decay nearly exponentially with decreasing  $V_3$ . In this regime, indeed,  $g_{DET}^T$  can be expressed as  $g_{DET}^T \sim \exp(-[E_0 - E_F]/\delta)$ . Importantly,  $I_{CF}$  decays much slower than  $g_{DET}^T$ , which is readily seen from the data for most negative  $V_3$ . This means that electrons excited well above  $E_F$  are responsible for the counterflow in the pinch-off regime, i.e.  $I_{CF} \sim \exp(-[E_0 - E_F - E^*]/\delta)$ , where  $E^*$  is their characteristic excess energy. Standard gate voltage to energy calibration gives an estimate of  $E^* \sim 0.5$  meV (see the scale bar in figure 5(b) corresponding to  $\Delta E_0 \approx 1$  meV). The thermoelectric model fails to simultaneously account for the energy scale  $E^*$  and measured  $I_{CF}$  values<sup>5</sup>. A lead temperature difference of about 3 K would be needed in the former case, which corresponds to thermal currents two orders of magnitude higher than actually measured (peak values  $\sim 10$  nA versus  $\sim 100$  pA in figure 4). Hence, the above analysis shows that the distribution function of electrons in one of the detector leads is strongly non-thermal, out-weighted towards high excitation energies compared to the usual Fermi–Dirac distribution. The nonequilibrium distribution function is a result of continuous drive-QPC-mediated excitation of a 2DEG region next to the detector-QPC and its continuous cooling via interchange of electrons with neighbouring cold 2DEG regions. This process is accompanied by a non-zero counterflow current across the detector-QPC thanks to the above-mentioned energy dependence of its transmission probability.

A rough test for a spatial extent of the excited 2DEG region can be performed by using gates 6 or 10 (instead of gate 8) to define the drive-QPC (figure 1(a)). We have checked [10] that, despite the resulting mutual shift of the drive and detector QPCs by about  $\pm 300$  nm along gate C, the counterflow effect is still observed for both directions of the drive current in each case, confirming the relevance of the 2DEG leads. Finally, the observed direction of the counterflow defines the following empirical rule. The nonequilibrium lead of the detector-QPC is the one neighbouring the drain lead of the drive-QPC, i.e. the lead with the lower electrochemical potential where the electrons are being injected (see figure 1(c)).

## 5. Excitation of a quantum dot with an isolated QPC

In the last sections we showed how a generation of current occurs in the DQD- and QPC-based detector circuits neighbouring the drive-QPC circuit. Here we demonstrate that

<sup>5</sup> We note that the saddle-point model [17] used is not fully consistent with the experimental dependence of  $G_{DET}$  on  $V_3$ . For example, a proportionality  $g_{DET}^T \propto T_0(1 - T_0)$  predicted by the model is not exactly fulfilled in our experiment (compare solid and dashed lines in figure 5(b)). Such minor discrepancies do not affect our conclusions about the relation between thermopower and counterflow.

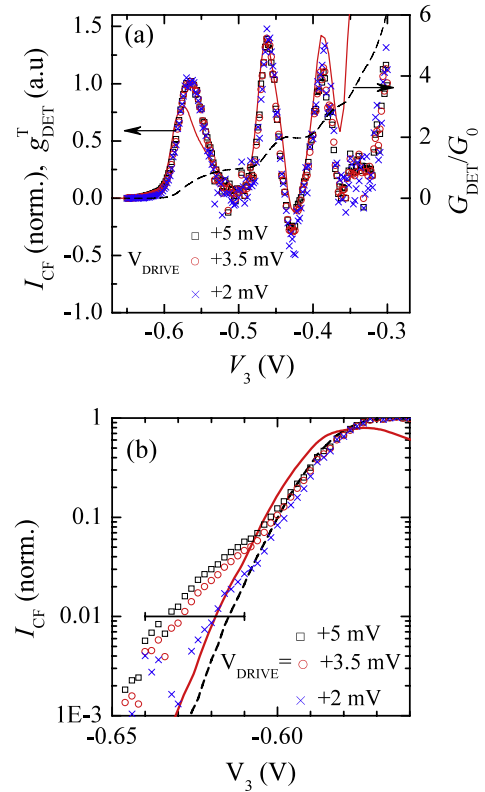


**Figure 5.** (a)  $I_{CF}$  versus  $V_3$  normalized by its left-most peak value for a set of  $V_{DRIVE}$  values (left panel). Conductance (dashed) and transconductance (solid line) of the detector-QPC (right panel). (b) Log scale of  $I_{CF}$  near detector pinch-off.  $g_{DET}^T$  (same units as in (a)) and transmission function  $T_0(1 - T_0)$  of the detector-QPC are also shown as solid and dashed lines, respectively. The bar indicates a gate voltage scale corresponding to a change of  $E_0 - E_F$  by 1 meV.

a nonequilibrium excitation with a drive-QPC also influences the conductance of a single QD in the detector circuit. The sketch of the experiment is shown in figure 1(d). At fixed  $V_{DRIVE}$  the differential QD conductance  $g_{DOT}$  is measured in the linear regime as a function of gate voltage  $V_2$ , which controls the dot's electrochemical potential. Throughout this section, again,  $g_{DRIVE} \approx 0.5 G_0$ .

In figure 6  $g_{DOT}$  is plotted versus  $V_2$  for one relatively small and two much higher values of  $|V_{DRIVE}|$ . At a small drive bias of 0.5 mV nonequilibrium excitation is ineffective (see the two previous sections) and  $g_{DOT}$  shows three usual Coulomb blockade peaks. Two Coulomb valleys between the peaks are marked with numbers  $N$  and  $N + 1$  corresponding to the (unknown) total number of QD electrons in each case. Each of these peaks corresponds to an equilibrium resonance condition, when the electrochemical potential of the QD aligns with that of the 2DEG leads ( $\mu_{LEADS}$ ). For instance, for the central peak this condition is  $E_{N+1}^g - E_N^g = \mu_{LEADS}$ , where  $E_N^g$  denotes the total energy of the ground  $N$ -electron state of the QD. At high  $|V_{DRIVE}|$  nonequilibrium excitation lifts the Coulomb blockade and  $g_{DOT}$  is strongly increased in Coulomb valleys (at least an order of magnitude). On top of a smooth background three resonant features are seen in Coulomb valleys in the presence of excitation (see arrows). These correspond to the transport through the excited states of the QD.

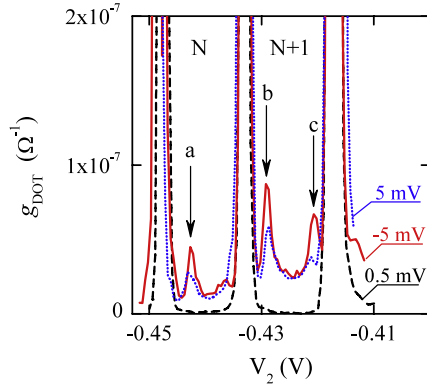


**Figure 6.** Differential conductance of the QD in the detector circuit versus gate voltage for three values of  $V_{\text{DRIVE}}$ . Three peaks in the Coulomb valleys (arrows a, b, c) correspond to conductance through excited QD states.

In the presence of excitation the QD is no longer at thermal equilibrium with its leads and its excited states are occupied with a probability much higher than that given by usual thermal fluctuations (exponentially small inside the Coulomb valley). In this case conductance peaks can be observed at different gate voltages, compared to the ground state resonances [1]. For example, if  $E_N^*$  denotes the total energy of the excited  $N$ -electron state, an extra conductance peak corresponds to the resonance condition  $E_N^* - E_{N-1}^g = \mu_{\text{LEADS}}$ . This peak is shifted to a more positive gate voltage compared to the ground state Coulomb blockade peak:  $\delta V_2 \propto (E_N^* - E_N^g)$ . Similarly, the extra peak for  $E_N^g - E_{N-1}^* = \mu_{\text{LEADS}}$  is shifted to a more negative gate voltage:  $\delta V_2 \propto -(E_{N-1}^* - E_{N-1}^g)$ . The resonances a/b/c in figure 6 correspond to a set of such nonequilibrium transitions  $\text{Ex}_N \leftrightarrow \text{Gr}_{N-1}/\text{Ex}_{N+1} \leftrightarrow \text{Gr}_N/\text{Ex}_{N+1} \leftrightarrow \text{Gr}_{N+2}$ , where Ex (Gr) stands for excited (ground) many-electron states. The excitation energies deduced from the peak positions equal  $E_N^* \approx 530 \mu\text{eV}$  and  $E_{N+1}^* \approx 340 \mu\text{eV}$ , respectively, for resonance a and resonances b and c.

Notably, only a few extra resonances are seen in figure 6 despite the bandwidth of the drive-QPC excitation far exceeding a single-particle level spacing in our QD ( $\sim 1 \text{ meV}$  versus  $\sim 100 \mu\text{eV}$ ). The reason why some resonances are most pronounced is probably related to optimal (maximal) ratio of the corresponding dot-lead tunnelling rate to the inelastic relaxation rate inside the dot. This idea can be directly verified by a measurement of the nonlinear differential conductance of the QD, where the excited states participate in transport thanks to a finite bias  $V_{\text{DOT}}$  across the QD. In figure 7 we show a colour-scale plot of  $g_{\text{DOT}}$  versus  $[V_2, V_{\text{DOT}}]$  in the absence of nonequilibrium excitation. Diamond-shaped regions of Coulomb blockade (Coulomb diamonds) are marked with corresponding electron numbers (same as in figure 6). X-shaped regions of finite conductance, centred at the positions of zero bias Coulomb peaks, correspond to a gate voltage range allowed for sequential tunnelling, which grows proportionally to  $|V_{\text{DOT}}|$ . At negative QD bias several lines of enhanced  $g_{\text{DOT}}$  are distinguished below  $N + 1$ th and  $N$ th Coulomb diamonds, which correspond to different excited

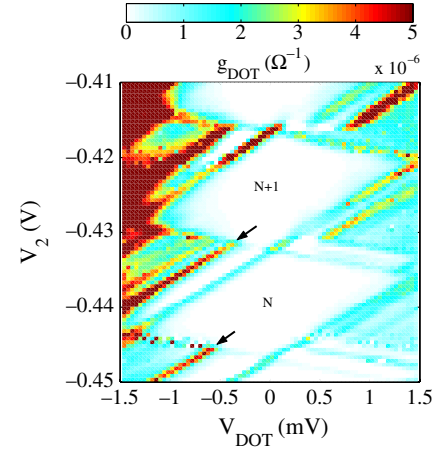


**Figure 7.** Colour-scale (grey-scale) plot of the QD's differential conductance in the absence of nonequilibrium excitation with the drive-QPC ( $V_{\text{DRIVE}} = 0.5 \text{ mV}$ ). Arrows indicate the two strongest source resonances corresponding to transport through  $N + 1$ -electron and  $N$ -electron excited QD states.

states participating in transport at bias voltages  $|V_{\text{DOT}}| > E^* - E^g$ . The strongest among these resonances (marked with arrows) indeed correspond to the same excited states which are responsible for the extra resonances in figure 6.

## 6. Discussion

In the above sections we demonstrated that the externally biased drive-QPC can provide a nonequilibrium excitation to the neighbouring quantum circuit. The excitation has a large bandwidth of  $\sim 1 \text{ meV}$  and can be detected with a QD, a DQD or a QPC placed in the detector circuit. In all three cases a common feature of the drive-QPC-mediated excitation is observed: the excitation possesses a threshold-like drive-bias dependence and is suppressed for  $V_{\text{DRIVE}} \lesssim 1 \text{ mV}$ . This and other main observations can be explained in terms of an acoustic-phonon-based energy transfer mechanism between the two quantum circuits. We start the discussion from the counterflow effect, which allows a qualitative argument based on the conservation laws.

The key ingredients necessary for the counterflow are (section 4): (i) absorption of energy quanta up to  $1 \text{ meV}$  by the free 2DEG electrons and (ii) preferential energy flow to one of the leads. The first requirement allows us to rule out a possible contribution of the photon-mediated energy transfer based on conservation laws. Direct Coulomb interaction between the electrons of coplanar 2DEGs in the drive and detector circuits also cannot account for the counterflow. The momentum transferred via Coulomb interaction is restricted by the minimum distance between the electrons  $|q| \leq 10^{-5} \text{ cm}^{-1}$  (gate C wider than  $100 \text{ nm}$ , see figure 1(a)), which is much smaller than the Fermi momentum  $k_F > 10^{-6} \text{ cm}^{-1}$ . Under such conditions only a forward Coulomb scattering can occur, i.e. a mutual scattering of the two electrons moving in the same direction in different circuits, which obviously cannot give rise to the counterflow.

Both the above conditions can be satisfied if electron–phonon interaction is taken into account. Thanks to its ballistic nature the current flowing across the drive-QPC results in injection of hot electrons above the Fermi energy into the drain lead, which leave unoccupied states (holes) below the Fermi energy in the source lead<sup>6</sup>. The drain electron and source hole excess energies (referred to the respective Fermi energies  $\epsilon_e^D = E - E_F^D > 0$  and  $\epsilon_h^S = E - E_F^S < 0$ ) satisfy  $\epsilon_e + |\epsilon_h| = |eV_{\text{DRIVE}}|$ . Energy relaxation of nonequilibrium carriers in the drive circuit can occur via emission of acoustic phonons. Part of the phonons with momenta parallel to the interface can be re-absorbed in the nearby detector circuit. Such phonons have momenta up to  $2\hbar k_F$  and energies up to  $2\hbar k_F v_s \approx 0.6$  meV (calculated for sound velocity  $v_s = 3 \times 10^5$  cm s<sup>-1</sup>) and can give rise to a strongly nonequilibrium distribution of electrons in the detector. Particularly important for the counterflow effect is a nonlinear transport regime across the drive-QPC near its pinch-off [10]. Here the excess energies of the injected drain electrons are much higher than those of the source holes  $\epsilon_h^S \ll \epsilon_e^D \approx |eV_{\text{DRIVE}}|$ , so that the emission of phonons in the drive circuit occurs preferably at the drain side [18]. Because of the device geometry (figure 1(a)), absorption of phonons in this case happens preferably in the neighbouring lead of the detector circuit. This naturally explains the origin of the asymmetric excitation responsible for the counterflow and the sign of this effect. Additional support for the above-discussed mechanism comes from the near-independence of the effect on the physical distance between the drive and detector-QPC, which was controlled by the voltage applied to gate C [11] (see the sketch of figure 1(c)).

Next we speculate how the acoustic-phonon-based energy transfer mechanism could explain our observations for the DQD quantum ratchet and QD excitation. In principle, high energy acoustic phonons can be directly absorbed by the localized QD electrons [9], which would suffice for a qualitative explanation. However, there exists an alternative microscopic mechanism. Strongly nonequilibrium electrons in the detector circuit create high frequency electric field fluctuations, which can in turn drive inelastic transitions in a QD and a DQD. In fact, the data of figures 2(c) and 6 look very similar to photon-assisted tunnelling data in DQD and QD under microwave excitation [7, 14]. An important hint in favour of the latter mechanism is the observation of the  $\Delta$ -independent and counterflow-like contribution to the drive-QPC-mediated current through the DQD [2]. Still, it is hard to unambiguously determine which of the two microscopic mechanisms is more relevant for the excitation of the DQD ratchet and the QD in our experiments.

While the spatial asymmetry of the excitation in the drive circuit, characteristic for the nonlinear transport regime, is relevant for the counterflow, it is not necessary for the QD and DQD ratchet experiments. Therefore one would naively expect the phonon-mediated excitation to be efficient also at small drive bias in the last two experiments. In contrast, we find that in all three cases the drive-QPC-mediated excitation

is suppressed for<sup>7</sup>  $|V_{\text{DRIVE}}| \lesssim 1$  mV (see, e.g., figure 2). Though it is hard to give a quantitative explanation for this onset, we simply attribute it to the steepness of the drive-bias dependence owing to a rapid decrease of an electron–phonon energy relaxation rate at small excess energies. In the so-called Bloch–Grüneisen limit a cooling power of the 2DEG can fall as  $P \sim T_e^3 - T_l^3$  or faster at low temperatures in a polar crystal like GaAs [19] ( $T_e, T_l$  are the electron and lattice temperatures). Hence a cooling power of the drive circuit falls at not too high a bias as  $P \sim \alpha^3 |V_{\text{DRIVE}}|^3$ , where  $\alpha \leq 1$  is a bias lever-arm coefficient, which defines the characteristic excess energy of the nonequilibrium carriers ( $\alpha = 1$  in the strongly nonlinear regime, see above). The average path length a nonequilibrium electron travels before emitting an acoustic phonon at small excess energies can exceed even the size of our whole device [19]. This should result in even steeper drive-bias dependence of the detector response, since a vanishingly small fraction of the phonons emitted in the drive circuit can be re-absorbed in the vicinity of the neighbouring detector nanostructure as  $|V_{\text{DRIVE}}|$  is decreased. In the end, we would like to point out that the above qualitative argument alone fails to fully explain some of our observations, e.g. the enhanced efficiency of the DQD ratchet excitation near the drive-QPC pinch-off (figure 3(a)). Possibly some properties of the drive-QPC in the nonlinear transport regime and/or an alternative mechanism of the energy transfer could be relevant here, see, for example, [20].

In conclusion, we studied the energy transfer from an externally biased drive circuit containing a drive-QPC to a neighbouring detector circuit containing a DQD, a QPC or a QD. In all three cases a 1 meV bandwidth excitation is observed, provided the drive bias is in the mV range. The main features of the experiments are explained within a qualitative model of acoustic-phonon-based energy transfer mechanism. Nonequilibrium acoustic phonons are emitted in the vicinity of the drive-QPC and re-absorbed in the 2DEG of the detector circuit. This mechanism is most efficient at high drive bias and near the drive-QPC pinch-off, which has to be considered in experiments on coupled quantum circuits.

## Acknowledgments

The authors are grateful to V T Dolgoplov, A W Holleitner, C Strunk, F Wilhelm, I Favero, A V Khaetskii, N M Chtchelkatchev, A A Shashkin, D V Shovkun and P Hänggi for valuable discussions and to D Schröer and M Kroner for technical help. We thank the DFG via SFB 631, the BMBF via DIP-H.2.1, the Nanosystems Initiative Munich (NIM) and VSK the A von Humboldt Foundation, RFBR, RSSF, RAS and the programme ‘The State Support of Leading Scientific Schools’ for support.

## References

- [1] Onac E, Balestro F, Willems van Beveren L H, Hartmann U, Nazarov Y V and Kouwenhoven L P 2006 *Phys. Rev. Lett.* **96** 176601

<sup>6</sup> Here we choose the source/drain to be the lead with the higher/lower electrochemical potential, so that  $\mu_{\text{DRIVE}}^S = \mu_{\text{DRIVE}}^D + |eV_{\text{DRIVE}}|$  (note the definition dependence on the sign of  $V_{\text{DRIVE}}$ ).

<sup>7</sup> Note that suppression of the excitation at low bias does not allow us to observe a minimum bias condition for single-quanta excitation at certain energy  $|V_{\text{DRIVE}}^{\text{min}}| \geq |E/e|$ , which was verified in shot-noise detection [1, 3].

- [2] Khrapai V S, Ludwig S, Kotthaus J P, Tranitz H P and Wegscheider W 2006 *Phys. Rev. Lett.* **97** 176803
- [3] Gustavsson S, Studer M, Leturcq R, Ihn T, Ensslin K, Driscoll D C and Gossard A C 2007 *Phys. Rev. Lett.* **99** 206804
- [4] Debray P *et al* 2001 *J. Phys.: Condens. Matter* **13** 3389  
Debray P *et al* 2002 *Semicond. Sci. Technol.* **17** R21
- [5] Gramila T J *et al* 1991 *Phys. Rev. Lett.* **66** 1216
- [6] Gantmakher V F and Levinson Y B 1987 *Carrier Scattering in Metals and Semiconductors* (Amsterdam: North-Holland)
- [7] Oosterkamp T H, Kouwenhoven L P, Koolen A E A, van der Vaart N C and Harmans C J P M 1997 *Phys. Rev. Lett.* **78** 1536
- [8] Aguado R and Kouwenhoven L P 2000 *Phys. Rev. Lett.* **84** 1986
- [9] Fedichkin L, Yanchenko M and Valiev K A 2000 *Nanotechnology* **11** 387
- [10] Khrapai V S, Ludwig S, Kotthaus J P, Tranitz H P and Wegscheider W 2007 *Phys. Rev. Lett.* **99** 096803
- [11] Khrapai V S, Ludwig S, Kotthaus J P, Tranitz H P and Wegscheider W 2008 *Physica E* **40** 995
- [12] Molenkamp L W *et al* 1992 *Phys. Rev. Lett.* **68** 3765  
van Houten H *et al* 1992 *Semicond. Sci. Technol.* **7** B215
- [13] Dzurak A S *et al* 1993 *J. Phys.: Condens. Matter* **5** 8055
- [14] van der Wiel W G *et al* 2003 *Rev. Mod. Phys.* **75** 1
- [15] Reimann P 2002 *Phys. Rep.* **361** 57  
Reimann P and Hänggi P 2002 *Appl. Phys. A: Mater. Sci. Process.* **75** 169  
Kohler S, Lehmann J and Hänggi P 2005 *Phys. Rep.* **406** 379
- [16] Kristensen A *et al* 2000 *Phys. Rev. B* **62** 10950
- [17] Büttiker M 1990 *Phys. Rev. B* **41** 7906 and references therein
- [18] Palevski A *et al* 1989 *Phys. Rev. Lett.* **62** 1776
- [19] Ridley B K 1991 *Rep. Prog. Phys.* **54** 169
- [20] Chudnovskiy A L 2007 arXiv:0710.2403v1